Experimental realization of high-dimensional quantum gates with ultrahigh fidelity and efficiency

Zhe Meng,* Wen-Qiang Liu,* Bo-Wen Song, Xiao-Yun Wang, An-Ning Zhang,† and Zhang-Qi Yin‡

Center for Quantum Technology Research and Key Laboratory of Advanced Optoelectronic Quantum Architecture and Measurements (MOE), School of Physics, Beijing Institute of Technology, Beijing 100081, China

(Received 29 November 2023; accepted 29 January 2024; published 20 February 2024)

Qudit, a high-dimensional quantum system, can provide a larger Hilbert space, and it has been shown that the larger Hilbert space has remarkable advantages over the smaller one in quantum information processing. However, it is a great challenge to realize the high-fidelity quantum gates with qudits. Here we theoretically propose and experimentally demonstrate the four-dimensional quantum gates (including the generalized Pauli X_4 gate, Pauli Z_4 gate, and all of their integer powers) with optical qudits based on the polarization-spatial degree of freedom of the single photon. Furthermore, we also realize the polarization-controlled eight-dimensional controlled-X_4 gate and all of its integer powers. The experimental results achieve both the ultrahigh average gate fidelity 99.73% and efficiency 99.47%, which are above the error threshold for fault-tolerant quantum computation. Our work paves the way for the large-scale high-dimensional fault-tolerant quantum computation with a polynomial resource cost.

DOI: 10.1103/PhysRevA.109.022612

I. INTRODUCTION

Quantum logic gates are essential building blocks in many quantum information processing tasks [1]. Some quantum gates, e.g., two-qubit controlled-NOT (CNOT) gates and some single-qubit gates, enable the construction of arbitrary quantum operations [2], which bridge a benchmark for routing to the large-scale universal quantum computation. In recent years, the realization of quantum gates in many physical platforms has attracted widespread attention and some interesting proposals have been theoretically developed and experimentally demonstrated [3–9].

In addition to the qubit, a qudit with d-ary ($d > 2$) digits has emerged as a richer resource in high-dimensional quantum systems and it has been extended to high-dimensional logic to encode and process quantum information [10,11]. Due to the larger size of the Hilbert space, quantum technologies based on qudits have shown their remarkable advantages over the ones in the smaller space. For example, the larger Hilbert spaces can be used to simplify quantum gates [12–15], improve the efficiency of fault-tolerant quantum computation [16,17], increase channel capacity [18–21], improve communication security [22–24], and so on. In addition, they can also exceed the limitations imposed by the smaller spaces in stronger violation of Bell-type inequality [25–27] and higher noise resilience [28–30]. Up to now, qudit-based quantum information processing has been reported and experimentally implemented in various physical systems [31–39]. Though quantum technologies with qudits have made significant progress, a lot of efforts still are required for improving the quantum gates fidelity [31,32].

The photon is a natural candidate for encoding the qudit due to its various degrees of freedom (DOFs). Recently, many hybrid quantum systems with multiple DOFs have been used in quantum information processing [40–45]. There are many experiments that have also been demonstrated in high-dimensional quantum gates for the qudits, which are formed by the orbital angular momentum (OAM) [46–49], the time-frequency DOF [50], or the spatial modes of photons [51,52]. In 2017, Babazadeh *et al.* the authors experimentally demonstrated a four-dimensional generalized Pauli X_4 gate and all of its integer powers with a conversion efficiency of 87.3% and a fidelity of 93.4% using the OAM mode of a single photon [46]. Later, Wang *et al.* improved the conversion efficiency to 93% [49]. In 2022, Chi *et al.* experimentally realized the Pauli X_4 gate with the fidelity of 98.8% and a controlled-X_4 gate with the fidelity of 95.2% on a programmable silicon-photonic quantum processor [52]. In all of the above works [46–49,52], the experimental realization of the high-dimensional quantum gates depends on either the multiple Sagnac-type interferometers or multiple Mach-Zehnder-type interferometers, which are both faced with the great challenges of phase instability. Therefore, the fidelity and efficiency of the high-dimensional quantum gates for the optical qudits are significantly degraded, compared to their qubit counterparts [53–55].

In this paper, we experimentally demonstrate the four-dimensional quantum gates on the single photons carrying both the polarization and the spatial mode DOFs. The gates include the four-dimensional Pauli X_4 gate, Pauli Z_4 gate, and all of their integer powers, which can efficiently construct any quantum operations in the four-dimensional state space [46]. The Pauli X_4 gate, Pauli Z_4 gate, and all of their integer powers are realized using the polarization-spatial DOF of the single photons. We also realize the polarization-controlled eight-dimensional controlled-X_4 gate and all of its integer powers. Our experiments simplify the previous works [46–49,52] and improve the phase stability. The experimental results

*These authors contributed equally to this work.
†Corresponding author: Anningzhang@bit.edu.cn
‡Corresponding author: zqyin@bit.edu.cn

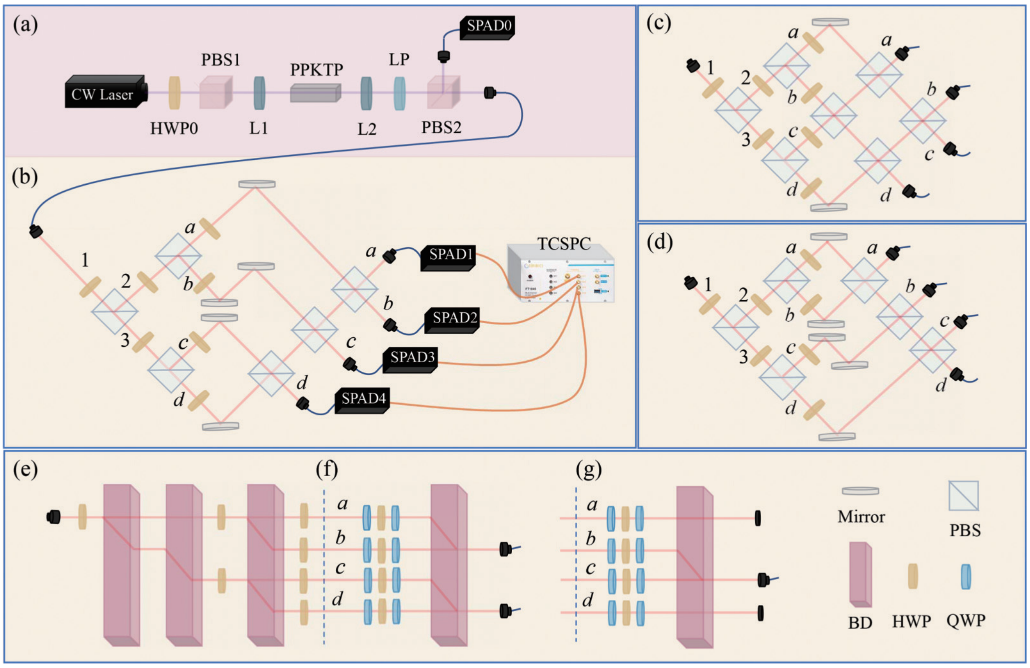

FIG. 1. Schematic of the experimental setup for realization of the generalized four-dimensional Pauli X_4 gate, Pauli Z_4 gate, and all of their integer powers. (a) The preparation of a heralded single-photon source. The experimental setups for the realization of (b) X_4 gate, (c) X_4^2 gate, and (d) $X_4^\dagger$ gate, where the optical elements before the mirrors present the initial state preparation and the optical elements after the mirrors describe the gate operations. (e)–(g) The experimental setups for the realization of Pauli Z_4, Z_4^2, $Z_4^\dagger$ gates. (e) The initial state preparation of the Z_4, Z_4^2, $Z_4^\dagger$ gates. (f)–(g) The implementation of the Pauli Z_4, Z_4^2, $Z_4^\dagger$ gates and the measurement of the phase differences in spatial modes a and b, c and d, b and c. The effective coincidence window (including the jitter of the detector) is about 2 ns.

show both ultrahigh (∼99.5%) gate efficiency and fidelity, which are above error threshold for fault-tolerant quantum computation [56,57].

II. HIGH-DIMENSIONAL QUANTUM GATES

A qudit quantum gate is described in a d-dimensional Hilbert space $\mathcal{H}_d$ that is spanned by a set of orthogonal bases $\{|0\rangle, |1\rangle, \ldots, |d-1\rangle\}$. The most important d-dimensional quantum gates are the generalized single-qudit Pauli X_d gate, Pauli Z_d gate, two-qudit controlled-X_d gate, and all their integer powers. The transformations of the d-dimensional single-qudit n (an integer number) powers of Pauli X_d (X_d^n) gate and n powers of Z_d (Z_d^n) gate on the d-dimensional quantum state are expressed by [58]

$$X_d^n|l\rangle = |l \oplus n\rangle_{\mathrm{mod}d}, \quad Z_d^n|l\rangle = \omega^{n\cdot l}|l\rangle. \tag{1}$$

Here $l \in \{0, 1, \ldots, d-1\}$, $|l \oplus n\rangle_{\mathrm{mod}d}=(l+n)$ modulo d, and $\omega=\exp(2\pi i/d)$. The X_d^n gate is a cyclic operation in which each quantum state is transformed to its nth nearest state in a clockwise direction. The Z_d^n gate is a phase operation in which each quantum state is introduced by a state-dependent phase. The generalized n powers of Pauli Y_d (Y_d^n) gate can be given by $Y_d^n = X_d^n Z_d^n$. When $n=1$ and $d=2$, they would simplify to the qubit Pauli X gate, Pauli Y gate, and Pauli Z gate. In addition, an important two-qudit gate is the controlled-X_d^n ($C_d X_d^n$) gate in a d^2-dimensional Hilbert space ($\mathcal{H}_d^c \otimes \mathcal{H}_d^t$), which is formulated as [11]

$$C_d X_d^n(|k\rangle|l\rangle) = |k\rangle|k \oplus l \oplus (n-1)\rangle_{\mathrm{mod}d}. \tag{2}$$

Here $\mathcal{H}_d^c$ and $\mathcal{H}_d^t$ denote the Hilbert spaces of the controlled qudit and the target qudit, respectively. The $C_d X_d^n$ gate realizes a cyclic operation on the target qudit $|l\rangle$ by manipulating the value of the controlled qudit $|k\rangle$ and leaves it unchanged on the controlled qudit. $|k\rangle$ and $|l\rangle$ are the d-dimensional quantum states in the Hilbert spaces $\mathcal{H}_d^c$ and $\mathcal{H}_d^t$, respectively. In the two-qubit version, the $C_d X_d^n$ gate becomes the well-known CNOT gate.

III. EXPERIMENTAL SETUP

Quantum gates X_4, X_4^2, $X_4^\dagger$ ($X_4^\dagger = X_4^3$) and Z_4, Z_4^2, $Z_4^\dagger$ ($Z_4^\dagger = Z_4^3$) are sufficient to construct arbitrary quantum operations in the four-dimensional state space [46]. The experimental setup for the realization of these elementary gates is shown in Fig. 1, where the gate qudit is encoded on the polarization-spatial DOF of the single photons, i.e., $|0\rangle \leftrightarrow |Ha\rangle$, $|1\rangle \leftrightarrow |Hb\rangle$, $|2\rangle \leftrightarrow |Hc\rangle$, and $|3\rangle \leftrightarrow |Hd\rangle$. The horizontally H-polarized DOF of photons controls the spatial mode DOF (a, b, c, d) of photons to route the photons into the corresponding logic gates by using some linear optical elements. Note that the polarization state of the biphotons can also be used to encode the qudit and process quantum information with high-dimensional Hilbert space [59–62].

Figure 1(a) illustrates a heralded single-photon source in which a continuous-wave diode laser (CW laser) is employed to generate a pump laser beam with a central wavelength of 405 nm and an output power of 20 mW. This pump laser is utilized for the production of photon pairs at a wavelength of 810 nm through type-II spontaneous parametric down-conversion in a periodically poled potassium titanyl phosphate (PPKTP) crystal. A half-wave plate (HWP0) and a polarization beam splitter (PBS1) are used to regulate optical power, and two lenses (L1 and L2) placed before and after the PPKTP crystal are used to focus and collimate beams. Then, the photon pairs are filtered at a long pass filter (LP) to eliminate any residual pumped laser light and they finally are split at PBS2. During this process, one photon from each pair is detected at the single-photon avalanche photodiode (SPAD0) to serve as a herald idler photon, and the other photon from pairs as signal photon H is injected into a four-dimensional Pauli X_4 gate in Fig. 1(b).

As shown in Fig. 1(b), the $|H\rangle$ photon first goes through a HWP in spatial mode 1 to evolve the H-polarized photon into the superposition of the horizontally H-polarized photon and vertically V-polarized photon. Then a PBS reflects the V-polarized photon into the spatial mode 2 and transmits the H-polarized photon into the spatial mode 3. Subsequently, the photons in spatial modes 2 and 3 go through HWPs, PBSs, and HWPs respectively, in which the PBSs divide the photons into the spatial modes a, b, c, d. Because the parameters of the HWPs can be adjusted arbitrarily, the four-dimensional Hilbert space is spanned by the trajectories of photons in a, b, c, and d, which generates a general superposition of polarization-spatial states (see Appendix A)

$$\alpha|Ha\rangle + \beta|Hb\rangle + \gamma|Hc\rangle + \delta|Hd\rangle. \tag{3}$$

Here the complex coefficients α, β, γ, and δ satisfy the normalization condition $|\alpha|^2 + |\beta|^2 + |\gamma|^2 + |\delta|^2 = 1$. After the initial state is prepared, the photon is routed to a X_4 gate that is composed of three PBSs, which evolves the initial state in Eq. (3) as

$$\alpha|Hb\rangle + \beta|Hc\rangle + \gamma|Hd\rangle + \delta|Ha\rangle. \tag{4}$$

From Eq. (3) to Eq. (4), one can see that the X_4 gate is accomplished. In this way, the X_4^2 gate and $X_4^\dagger$ gate also can be realized by routing the photon to different spatial modes using the PBSs, and the corresponding experimental setups are presented in Figs. 1(c) and 1(d), respectively.

Our four-dimensional quantum gates exhibit advantages over quantum walk. In our experiment, the X gate can transit from the spatial mode d to the spatial mode a using merely three PBSs. The quantum walk scheme requires three steps to complete, which is an operation that requires 15 PBSs and 30 HWPs. This is primarily due to the fact that the number of optical elements required for quantum walk increases polynomially with the number of steps. In the quantum walk scheme, a d-dimensional Pauli X_d gate and C_2X_d gate can be realized by using $(1.5d^2 - 2.5d + 1)$ PBSs and $(3d^2 - 5d + 2)$ HWPs [63–65].

We also experimentally realize the Pauli Z_4, Z_4^2, and $Z_4^\dagger$ gates shown in Figs. 1(e) to 1(g). Specifically, Fig. 1(e) presents the initial state preparation using the beam displacers (BDs) and HWPs, which can modeled as a general state in Eq. (3). In this case, it is equivalent to the method of using PBSs and HWPs for the initial state preparation of the X_4 gate. Figures 1(f) to 1(g) show the gate operations and the relative phase measurements, where a combination of two quarter-wave plates (QWPs) and one HWP is usd to introduce the state-dependent phase operations in corresponding spatial modes, and finally measuring the relative phase between two pairwise locations by the interference of the photons from the spatial modes a and b, c and d, b and c, respectively. Note that we utilize BD as a substitute for PBS in the realization of Z gates, which can improve the phase stability and the fidelity of Z gates. Due to the interchangeability of BD and PBS in linear optical systems, it becomes feasible to implement all U(4) unitaries using PBS within our established framework.

TABLE I. The in-out efficiency $\mathcal{P}(i, j)$ for the X_4, X_4^2, and $X_4^\dagger$ gates in our experimental setups.

Input mode	$\|Ha\rangle$	$\|Hb\rangle$	$\|Hc\rangle$	$\|Hd\rangle$
X_4 gate	99.58%	99.13%	99.60%	99.31%
X_4^2 gate	99.19%	99.84%	99.96%	99.46%
$X_4^\dagger$ gate	99.33%	99.81%	99.77%	99.11%

In experiments, the output signal photons after the gate operations are detected by a measurement device consisting of four SPADs (SPAD1, SPAD2, SPAD3, SPAD4) and a time-correlated single photon counting (TCSPC). This allows the photon number statistics in each output spatial modes to count the probabilities of all four elementary output bases for the Pauli X_4, X_4^2, $X_4^\dagger$ gates, and it also ascertains the relative phases between pairwise output spatial modes for the Pauli Z_4, Z_4^2, $Z_4^\dagger$ gates. This measurement process is sustained over a duration of 10 seconds by registering the coincidence between the SPAD1, SPAD2, SPAD3, SPAD4 and triggering SPAD0, respectively. For each measurement, we record the detection of approximately 9000 heralded single photons by registering the clicks over a duration of 1 second.

IV. EXPERIMENTAL RESULTS

The conversion efficiency and gates fidelity can be used to evaluate the performance of the quantum gates. The conversion efficiency of the gate is defined as $\mathcal{P}(i, j) = n_{ij}/\sum_k n_{ik}$. Here n_{ij} denotes the output photon number in the jth spatial mode when the input photon is in the ith spatial mode, and $\sum_k n_{ik}$ denotes the summation over the photon number in all possible output spatial modes when the input photon is in the ith spatial mode. We reconstruct the truth tables for the X_4, X_4^2, and $X_4^\dagger$ gates plotted in Fig. 2, which describe the population of all computational basis output states to each of the computational basis input states. We calculate the efficiencies of the X_4, X_4^2, and $X_4^\dagger$ gates and list them in Table I. The average efficiencies of the X_4, X_4^2, and $X_4^\dagger$ gates are 99.41%, 99.61%, 99.50%, respectively.

To check the transformations are quantum gates instead of classical gates, we need to input the four-dimensional state in a quantum superposition way. In experiments, we send the photons prepared in an equal superposition state into the gate operations and then measure the output state. We calculate the gate fidelity $\mathcal{F}(\rho_e, \rho_t) = \mathrm{Tr}(\sqrt{\sqrt{\rho_e}\rho_t\sqrt{\rho_e}})$ between the experimental output state ρ_e and the theoretical output state $\rho_t = U\rho_i U^\dagger$ (ρ_i is input sate and U is the transformation of the gates) [1]. We find that the fidelities for X_4, X_4^2, and $X_4^\dagger$ gates are $\mathcal{F}_{X_4} = 99.70\%$, $\mathcal{F}_{X_4^2} = 99.80\%$, and $\mathcal{F}_{X_4^\dagger} = 99.75\%$, which significantly go beyond the maximum fidelity for these

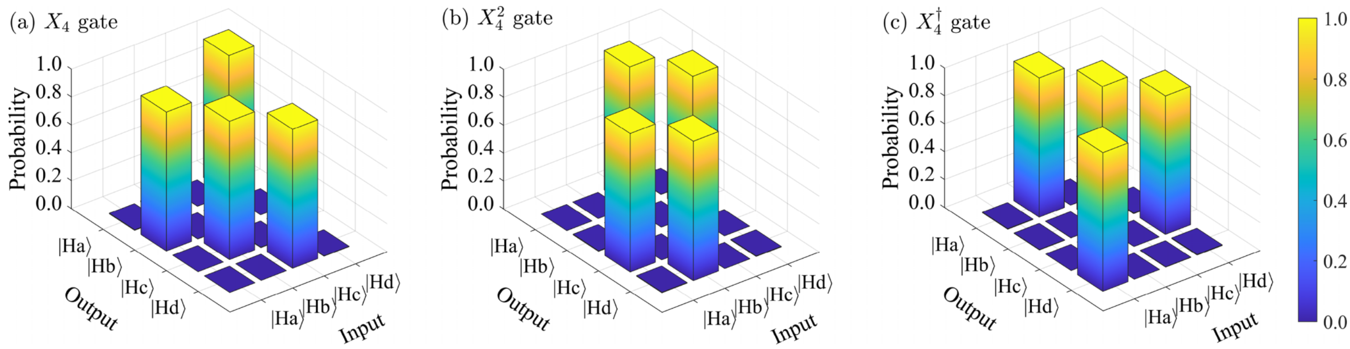

FIG. 2. Truth tables for (a) X_4 gate, (b) X_4^2 gate, and (c) $X_4^\dagger$ gate. After preparing a qudit in one of the four input computational basis from $|Ha\rangle$ to $|Hd\rangle$, the probabilities of all output basis states are measured in tens. The average conversion efficiencies of truth tables for X_4 gate, X_4^2 gate and $X_4^\dagger$ gate are 0.9941, 0.9961, and 0.9950, respectively.

classical gates bounded by $\mathcal{F}_{\rm cl} = 49.82\%$ in our experiments [46]. These results suggest the gates run with ultrahigh quality in a coherent way and it can also obtain the similar outcome for the other possible coherent superpositions.

We experimentally demonstrate the state-dependent phase gates and illustrate the quality of these gates. Figure 3 shows the experimental density matrix for the Z_4 gate in an input equal superposition state, where the real and imaginary parts are reconstructed in Figs. 3(a) and 3(b), respectively. The density matrices for the Z_4^2 gate and $Z_4^\dagger$ gate can be found in Appendix B. We obtain the fidelity of the Z_4, Z_4^2, and $Z_4^\dagger$ gates $\mathcal{F}_{Z_4} = 99.81\%$, $\mathcal{F}_{Z_4^2} = 99.55\%$, and $\mathcal{F}_{Z_4^\dagger} = 99.83\%$. The experimental results of these quantum logic gates are in good agreement with the theoretical expectations.

It is a great challenge to realize the two-qudit controlled gates because the d^2-dimensional Hilbert space $(\mathcal{H}_d^c \otimes \mathcal{H}_d^t)$ is involved. We note that our experiments can realize the controlled-cyclic gates in a $2d$-dimensional Hilbert space $(\mathcal{H}_2^c \otimes \mathcal{H}_d^t)$ where the controlled qubit is in a two-dimensional Hilbert space $\mathcal{H}_2^c$ and the target qudit is in a d-dimensional Hilbert space $\mathcal{H}_d^c$. Specifically, the experimental setup in the Figs. 1(a) to 1(d) can realize the polarization-controlled eight-dimensional CX_4^n gates (we denote $C_2X_4^n$ as CX_4^n) and all of its integer powers by adjusting the angles of the HWPs for the initial state preparation. The controlled qubit of the CX_4^n gate is encoded on the polarization states and the target qudit is encoded on the spatial mode states. The CX_4^n gate in an eight-dimensional hybrid Hilbert space is expressed by

$$CX_4^n = |V\rangle\langle V| \otimes I_4 + |H\rangle\langle H| \otimes X_4^n. \tag{5}$$

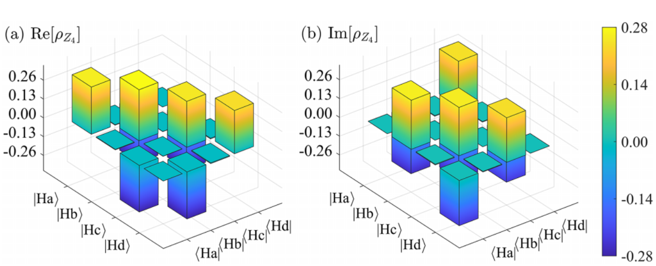

FIG. 3. The reconstructed density matrix ρ_{Z_4} for the Z_4 gate. (a), (b) are the real part and the imaginary part of the density matrix for the Z_4 gate, respectively. The fidelity of the Z_4 gate is 99.81%.

Here I_4 is a four-dimensional identical operation. When the controlled qubit is a V-polarized photon, the CX_4^n gate preforms an I_4 operation and when the controlled qubit is an H-polarized photon, the CX_4^n gate preforms an X_4^n operation. We initiate the preparation of a qudit in one of the eight elementary basis input states from $|Va\rangle, \ldots, |Vd\rangle, |Ha\rangle, \ldots, |Hd\rangle$, and execute a measurement procedure to count the probabilities of all eight elementary output states. The experimental truth table of the CX_4 gate is presented in Fig. 4 with an average conversion efficiency of 99.25%. The average efficiencies of the CX_4^2 and $CX_4^\dagger$ gates are 99.56% and 99.47%, and their truth tables can be found in Appendix C. We also obtain the fidelities for all these gates in an equal superposition input state, which are given by $\mathcal{F}_{CX_4} = 99.62\%$, $\mathcal{F}_{CX_4^2} = 99.78\%$, and $\mathcal{F}_{CX_4^\dagger} = 99.73\%$. The experimental errors mainly stem from the imperfections of the single-photon source, wave plates, and the photon detectors.

V. CONCLUSION

We investigated the implementations of four-dimensional generalized Pauli X_4 gate, Z_4 gate, and all of their integer powers based on the polarization-spatial DOF of the single photon. These quantum gates can construct arbitrary four-dimensional

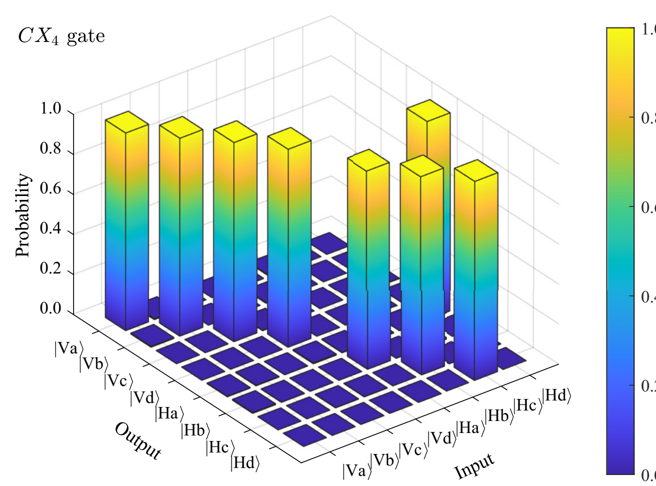

FIG. 4. Truth tables for the CX_4 gate. The average efficiency of the CX_4 gate is 99.25%.

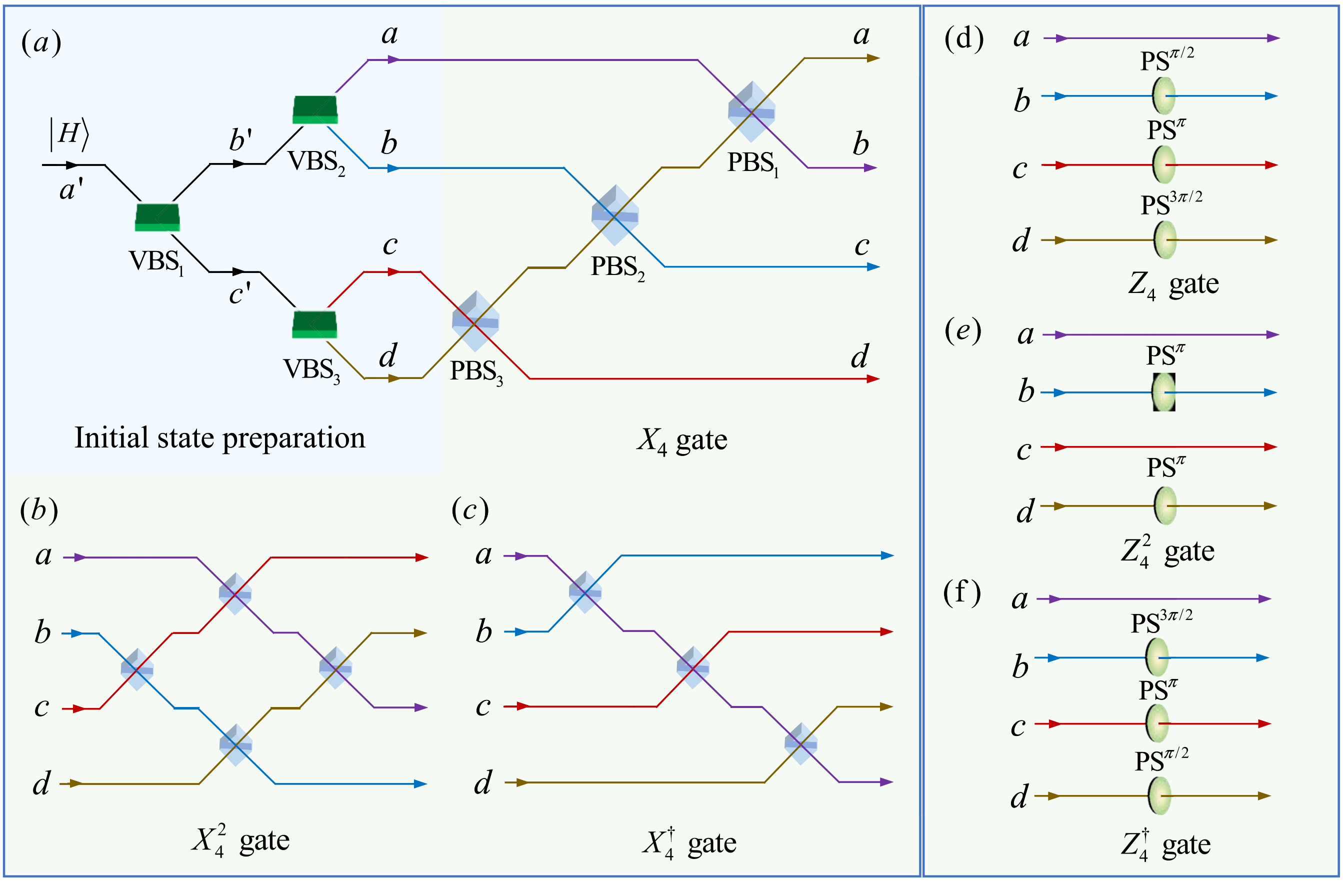

FIG. 5. Schematic proposals for realizing the four-dimensional Pauli X_4 gate, Z_4 gate, and all of their integer powers. (a) The initial state preparation and the realization of the X_4 gate. A horizontally polarized photon $|H\rangle$ is injected in the spatial mode a' to prepare a general initial state by using three spatial variable beam splitters (VBSs). Then the photon is routed to a X_4 gate composed of three polarized beam splitters (PBSs). The PBSs change the spatial mode of the incident photon from ($|Ha\rangle$, $|Hb\rangle$, $|Hc\rangle$, $|Hd\rangle$) to ($|Hb\rangle$, $|Hc\rangle$, $|Hd\rangle$, $|Ha\rangle$) because each PBS transmits the H-polarized photon and reflects the vertically V-polarized photon. (b) The realization of the X_4^2 gate where the spatial mode of the photon is changed from ($|Ha\rangle$, $|Hb\rangle$, $|Hc\rangle$, $|Hd\rangle$) to ($|Hc\rangle$, $|Hd\rangle$, $|Ha\rangle$, $|Hb\rangle$). (c) The realization of the $X_4^\dagger$ gate where the spatial mode of the photon is changed from ($|Ha\rangle$, $|Hb\rangle$, $|Hc\rangle$, $|Hd\rangle$) to ($|Hd\rangle$, $|Ha\rangle$, $|Hb\rangle$, $|Hc\rangle$). (d) The realization of the Z_4 gate. (e) The realization of the Z_4^2 gate. (f) The realization of the $Z_4^\dagger$ gate. PS$^\theta$ denotes a phase shifter with the angle θ, which introduces a mode-dependent phase $e^{i\theta}$ in the corresponding spatial modes.

quantum operations [46]. In addition, we also realized the polarization-controlled CX_4^n gates. Our experimental setups greatly simplified the implementations of these gates and the experimental results showed both the ultrahigh fidelity and efficiency, which improves significantly the previous works based on OAM [46–49].

These elementary high-dimensional quantum gates have important applications in many high-dimensional quantum information processing tasks, such as the preparation of high-dimensional entangled states [66], high-dimensional quantum key distribution [67], high-dimensional quantum teleportation [68], and quantum information transfer [69]. Our experiments can easily scale up more spatial modes to realize any higher-dimensional quantum operations. In this way, a d-dimensional Pauli X_d gate and CX_d gate can be realized by using $d-1$ PBSs, and a d-dimensional Pauli Z_d gate can be realized by using d HWPs and $2d$ QWPs. The work opens up a way to construct a large-scale qudit-based photonic chip quantum processor with a polynomial resource cost [52].

ACKNOWLEDGMENTS

This work is supported by National Natural Science Foundation of China (Grant No. 92365115), Beijing Institute of Technology Research Fund Program for Young Scholars.

APPENDIX A: PROPOSALS FOR THE REALIZING OF THE FOUR-DIMENSIONAL X_4 GATE, Z_4 GATE, AND ALL OF THEIR INTEGER POWERS

Figure 5 shows the theoretical proposals for realizing the four-dimensional Pauli X_4 gate, Z_4 gate, and all of their integer powers by encoding the gate qudit on the polarization-spatial degree of freedom of the single photons, i.e., $|0\rangle \leftrightarrow |Ha\rangle$, $|1\rangle \leftrightarrow |Hb\rangle$, $|2\rangle \leftrightarrow |Hc\rangle$, and $|3\rangle \leftrightarrow |Hd\rangle$. Here H is the horizontally polarized state of photons and a, b, c, d are the spatial modes of the photon. As shown in Fig. 5(a), a horizontally polarized photon $|H\rangle$ is injected into the spatial mode a' to prepare the initial state. The $|Ha'\rangle$ photon first goes through a variable beam splitter (VBS$_1$) to be divided into two arms b'

TABLE II. The angles of the wave plates group to achieve the relative phase in our experimental setups.

Phase $e^{i\theta}$	QWP1	HWP1	QWP2
$\theta = 0$	0°	0°	0°
$\theta = \pi/2$	90°	0°	0°
$\theta = \pi$	0°	90°	0°
$\theta = 3\pi/2$	90°	90°	0°

and c', which evolves the photon state as

$$|Ha'\rangle \rightarrow r_1|Hb'\rangle + t_1|Hc'\rangle. \tag{A1}$$

Here the coefficients r_1 and t_1 are determined by the reflectivity and the transmittance of the VBS_1, respectively, and they satisfy $|r_1|^2 + |t_1|^2 = 1$. The photons in spatial modes b' and modes c' are transmitted and reflected at VBS_2 and VBS_3 to span a four-dimensional Hilbert space in spatial modes a, b, c, and d. The VBS_2 and VBS_3 change the state in Eq. (A1) as

$$r_1|Hb'\rangle + t_1|Hc'\rangle \rightarrow r_1t_2|Ha\rangle + r_1r_2|Hb\rangle + t_1r_3|Hc\rangle + t_1t_3|Hd\rangle. \tag{A2}$$

Here the coefficients r_2, r_3, t_2, and t_3 are determined by the reflectivity and the transmittance of the VBS_2 and VBS_3, respectively, and they satisfy $|r_2|^2 + |t_2|^2 = |r_3|^2 + |t_3|^2 = 1$. Because the reflectivity and the transmittance of the VBS_1, VBS_2, and VBS_3 can be adjusted arbitrarily [70], we denote $\alpha = r_1t_2$, $\beta = r_1r_2$, $\gamma = t_1r_3$, and $\delta = t_1t_3$, then Eq. (A2) is rewritten as

$$|\varphi_1\rangle = \alpha|Ha\rangle + \beta|Hb\rangle + \gamma|Hc\rangle + \delta|Hd\rangle. \tag{A3}$$

Therefore, the initial state preparation is completed. In Figs. 1(b) to 1(d) of the experimental setups in the main text, we realize the same functionality as VBS by using a combination of HWP, PBS, and HWP. The HWPs positioned before the PBS serve to modulate the polarization according to coefficients r_1 and t_1. This modulation is mathematically represented as $|H\rangle \rightarrow \cos 2\theta|H\rangle + \sin 2\theta|V\rangle$, $|V\rangle \rightarrow \sin 2\theta|H\rangle - \cos 2\theta|V\rangle$, where θ signifies the angle of the optical axis of the HWP. Given that the PBS reflects the V-polarized photon and transmits the H-polarized photon, it can differentiate between the spatial modes of photons based on the ratio of H and V components. The HWP positioned after the PBS then transforms the polarization states of different

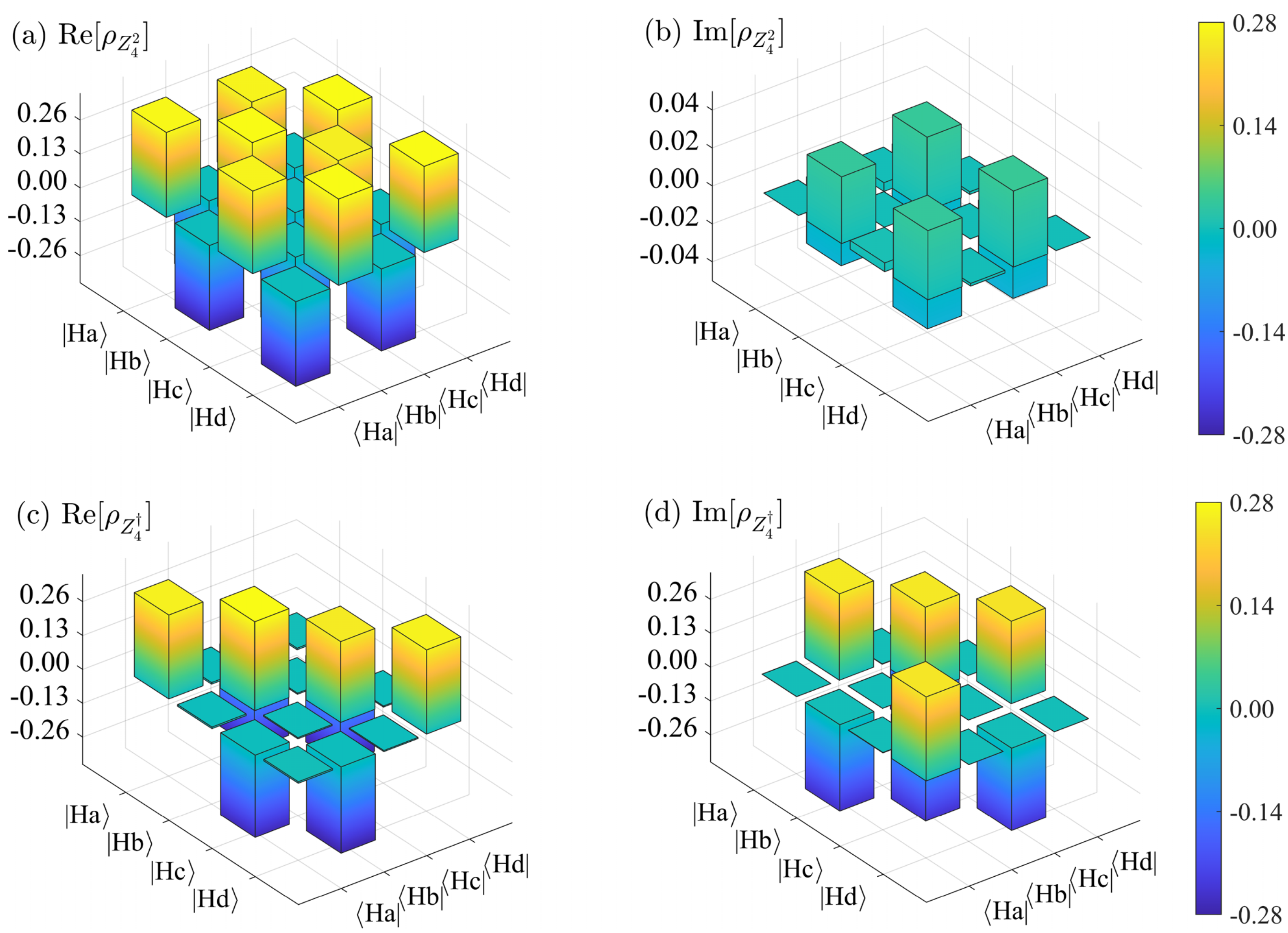

FIG. 6. The reconstructed density matrices $\rho_{Z_4^2}$ and $\rho_{Z_4^\dagger}$ for the Z_4^2 gate and $Z_4^\dagger$ gate, respectively. (a), (b) are the real part and the imaginary part of the density matrix for the Z_4^2 gate, respectively. (c), (d) are the real part and the imaginary part of the density matrix for the $Z_4^\dagger$ gate, respectively. The fidelities of the Z_4^2 gate and $Z_4^\dagger$ gate are 99.55% and 99.83%, respectively.

TABLE III. The in-out efficiency $\mathcal{P}(i, j)$ for the CX_4, CX_4^2, and $CX_4^\dagger$ gates in our experimental setups.

Input mode	$\|Va\rangle$	$\|Vb\rangle$	$\|Vc\rangle$	$\|Vd\rangle$	$\|Ha\rangle$	$\|Hb\rangle$	$\|Hc\rangle$	$\|Hd\rangle$
CX_4 gate	98.95%	99.10%	99.70%	99.10%	99.19%	99.12%	99.56%	99.30%
CX_4^2 gate	99.03%	99.92%	99.61%	99.49%	99.19%	99.84%	99.96%	99.45%
$CX_4^\dagger$ gate	99.30%	99.88%	99.47%	99.42%	99.32%	99.79%	99.50%	99.09%

spatial modes into the same H polarization, thereby fulfilling the role of a VBS.

The complex coefficients α, β, γ, and δ are determined by the reflectivity and the transmittance of the VBSs and satisfy the normalization condition $|\alpha|^2 + |\beta|^2 + |\gamma|^2 + |\delta|^2 = 1$. After the initial state is prepared, the photon is routed to an X_4 gate that is composed of three polarized beam splitters (PBS_1, PBS_2, and PBS_3). Because the PBS transmits H-polarized photon and reflects vertically V-polarized photon, the PBS_1, PBS_2, and PBS_3 evolve the initial state as

$$|\varphi_1\rangle \rightarrow \alpha|Hb\rangle + \beta|Hc\rangle + \gamma|Hd\rangle + \delta|Ha\rangle = |\varphi_{X_4}\rangle. \quad \text{(A4)}$$

From Eq. (A3) to Eq. (A4), one can see that Fig. 5(a) realizes a X_4 gate. In this way, the X_4^2 gate and $X_4^\dagger$ gate also can be realized by routing the photon to corresponding spatial modes using the PBSs, and the corresponding proposals are presented in Figs. 5(b) and 5(c), respectively.

The proposals for realizing the Z_4, Z_4^2, $Z_4^\dagger$ gates are shown in Figs. 5(d) to 5(f), respectively. To realize these mode-dependent phase gates, we set some phase shifters (PS^θ) rotated to an angle θ in the spatial modes to introduce a relative phase $e^{i\theta}$. As shown in Fig. 5(d), three phase shifters with the angles $\frac{\pi}{2}$, π, and $\frac{3\pi}{2}$ are placed respectively in the modes b, c, and d to realize the Z_4 gate. After the photon goes through three PSs, the initial state in Eq. (3) is changed as

$$|\varphi_1\rangle \rightarrow \alpha|Hb\rangle + i\beta|Hc\rangle - \gamma|Hd\rangle - i\delta|Ha\rangle = |\varphi_{Z_4}\rangle. \quad \text{(A5)}$$

In this way, the X_4^2 gate and $X_4^\dagger$ gate also can be realized and they are presented in Figs. 5(e) and 5(f), respectively. In Figs. 1(f) to 1(g) of the experimental setups in the main text, we use the sandwich structure of the wave plates group QWP1-HWP1-QWP2 to realize the PSs. The angles of the wave plates group required to achieve PS are presented in Table II.

APPENDIX B: RECONSTRUCTED DENSITY MATRICES FOR THE Z_4^2 GATE AND $Z_4^\dagger$ GATE

To assess the relative phase imparted by the Z_4^2 gate and $Z_4^\dagger$ gate, we introduce an initial state $|\varphi\rangle = 1/2(|Ha\rangle + |Hb\rangle + |Hc\rangle + |Hd\rangle)$. We subsequently perform interferometry measurements on the spatial modes in pairs, such as a and b, c and d, b and c. The relative phase between two spatial modes is measured by the probability $P = 1/2(1 + \cos\theta)$ obtained from these measurements. In this way, we measure the experimental coefficients α, β, γ, δ by the interference of photons in spatial modes a and b, c and d, b and c for a input equal superposition state and plot the reconstructed density matrices for the Z_4^2 gate and $Z_4^\dagger$ gate in Fig. 6. The fidelities of the Z_4^2 gate and $Z_4^\dagger$ gate are 99.55% and 99.83%, respectively.

APPENDIX C: PERFORMANCE OF THE CX_4 GATE, CX_4^2 GATE, AND $CX_4^\dagger$ GATE

We check the conversion efficiencies of the CX_4 gate, CX_4^2 gate, and $CX_4^\dagger$ gate by preparing a qudit in one of the eight input computational basis $|Va\rangle, \ldots, |Vd\rangle, |Ha\rangle, \ldots, |Hd\rangle$. The probabilities of all output basis states are measured in tens. The results of the conversion efficiencies are presented in Table III and the truth tables of them are plotted in Fig. 7. The average efficiencies of the CX_4^2 gate and $CX_4^\dagger$ gate are 99.78% and 99.73%, respectively.

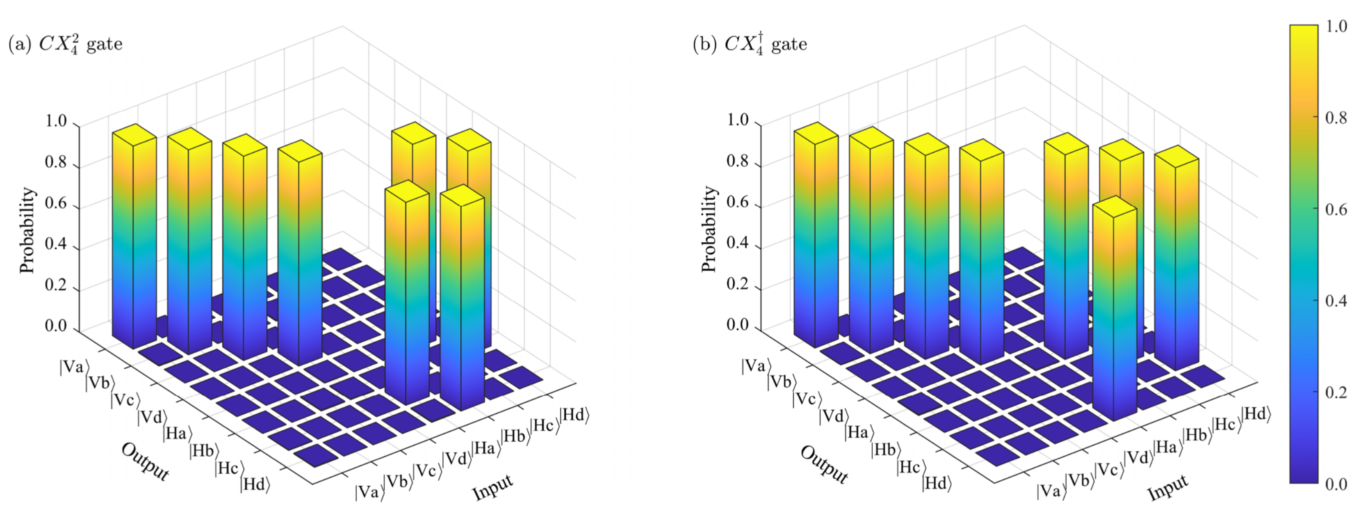

FIG. 7. Truth tables for the (a) CX_4^2 gate and (b) $CX_4^\dagger$ gate. The average efficiencies of the CX_4^2 gate and $CX_4^\dagger$ gate are 99.78% and 99.73%, respectively.

[1] M. A. Nielsen and I. L. Chuang, *Quantum Computation and Quantum Information* (Cambridge University Press, Cambridge, England, 2010).
[2] A. Barenco, C. H. Bennett, R. Cleve, D. P. DiVincenzo, N. Margolus, P. Shor, T. Sleator, J. A. Smolin, and H. Weinfurter, Elementary gates for quantum computation, Phys. Rev. A **52**, 3457 (1995).
[3] E. Knill, R. Laflamme, and G. J. Milburn, A scheme for efficient quantum computation with linear optics, Nature (London) **409**, 46 (2001).
[4] J. L. O'Brien, G. J. Pryde, A. G. White, T. C. Ralph, and D. Branning, Demonstration of an all-optical quantum controlled-NOT gate, Nature (London) **426**, 264 (2003).
[5] Z. Zhao, A. N. Zhang, Y. A. Chen, H. Zhang, J. F. Du, T. Yang, and J. W. Pan, Experimental demonstration of a nondestructive controlled-NOT quantum gate for two independent photon qubits, Phys. Rev. Lett. **94**, 030501 (2005).
[6] J. Zeuner, A. N. Sharma, M. Tillmann, R. Heilmann, M. Gräfe, A. Moqanaki, A. Szameit, and P. Walther, Integrated-optics heralded controlled-NOT gate for polarization-encoded qubits, npj Quantum Inf. **4**, 13 (2018).
[7] J. P. Li, X. Gu, J. Qin, D. Wu, X. You, H. Wang, C. Schneider, S. Höfling, Y. H. Huo, C. Y. Lu, N. L. Liu, L. Li, and J. W. Pan, Heralded nondestructive quantum entangling gate with single-photon sources, Phys. Rev. Lett. **126**, 140501 (2021).
[8] W. Q. Liu, H. R. Wei, and L. C. Kwek, Universal quantum multi-qubit entangling gates with auxiliary spaces, Adv. Quantum Technol. **5**, 2100136 (2022).
[9] W. Q. Liu and H. R. Wei, Linear optical universal quantum gates with higher success probabilities, Adv. Quantum Technol. **6**, 2300009 (2023).
[10] M. Luo and X. Wang, Universal quantum computation with qudits, Sci. China Phys. Mech. Astron. **57**, 1712 (2014).
[11] Y. Wang, Z. Hu, B. C. Sanders, and S. Kais, Qudits and high-dimensional quantum computing, Front. Phys. **8**, 589504 (2020).
[12] T. C. Ralph, K. J. Resch, and A. Gilchrist, Efficient Toffoli gates using qudits, Phys. Rev. A **75**, 022313 (2007).
[13] B. P. Lanyon, M. Barbieri, M. P. Almeida, T. Jennewein, T. C. Ralph, K. J. Resch, G. J. Pryde, J. L. O'Brien, A. Gilchrist, and A. G. White, Simplifying quantum logic using higher-dimensional Hilbert spaces, Nat. Phys. **5**, 134 (2009).
[14] W. Q. Liu and H. R. Wei, Optimal synthesis of the Fredkin gate in a multilevel system, New J. Phys. **22**, 063026 (2020).
[15] W. Q. Liu, H. R. Wei, and L. C. Kwek, Low-cost Fredkin gate with auxiliary space, Phys. Rev. Appl. **14**, 054057 (2020).
[16] E. T. Campbell, Enhanced fault-tolerant quantum computing in d-level systems, Phys. Rev. Lett. **113**, 230501 (2014).
[17] M. Howard and E. Campbell, Application of a resource theory for magic states to fault-tolerant quantum computing, Phys. Rev. Lett. **118**, 090501 (2017).
[18] H. Bechmann-Pasquinucci and W. Tittel, Quantum cryptography using larger alphabets, Phys. Rev. A **61**, 062308 (2000).
[19] J. Cortese, Holevo-Schumacher-Westmoreland channel capacity for a class of qudit unital channels, Phys. Rev. A **69**, 022302 (2004).
[20] P. B. Dixon, G. A. Howland, J. Schneeloch, and J. C. Howell, Quantum mutual information capacity for high-dimensional entangled states, Phys. Rev. Lett. **108**, 143603 (2012).
[21] X. M. Hu, Y. Guo, B. H. Liu, Y. F. Huang, C. F. Li, and G. C. Guo, Beating the channel capacity limit for superdense coding with entangled ququarts, Sci. Adv. **4**, eaat9304 (2018).
[22] N. J. Cerf, M. Bourennane, A. Karlsson, and N. Gisin, Security of quantum key distribution using d-level systems, Phys. Rev. Lett. **88**, 127902 (2002).
[23] L. Zhang, C. Silberhorn, and I. A. Walmsley, Secure quantum key distribution using continuous variables of single photons, Phys. Rev. Lett. **100**, 110504 (2008).
[24] F. Wang, P. Zeng, J. Zhao, B. Braverman, Y. Zhou, M. Mirhosseini, X. Wang, H. Gao, F. Li, R. W. Boyd, and P. Zhang, High-dimensional quantum key distribution based on mutually partially unbiased bases, Phys. Rev. A **101**, 032340 (2020).
[25] D. Collins, N. Gisin, N. Linden, S. Massar, and S. Popescu, Bell inequalities for arbitrarily high-dimensional systems, Phys. Rev. Lett. **88**, 040404 (2002).
[26] T. Vértesi, S. Pironio, and N. Brunner, Closing the detection loophole in Bell experiments using qudits, Phys. Rev. Lett. **104**, 060401 (2010).
[27] A. C. Dada, J. Leach, G. S. Buller, M. J. Padgett, and E. Andersson, Experimental high-dimensional two-photon entanglement and violations of generalized Bell inequalities, Nat. Phys. **7**, 677 (2011).
[28] L. Sheridan and V. Scarani, Security proof for quantum key distribution using qudit systems, Phys. Rev. A **82**, 030301(R) (2010).
[29] Z. Liu and H. Fan, Decay of multiqudit entanglement, Phys. Rev. A **79**, 064305 (2009).
[30] S. Ecker, F. Bouchard, L. Bulla, F. Brandt, O. Kohout, F. Steinlechner, R. Fickler, M. Malik, Y. Guryanova, R. Ursin, and M. Huber, Overcoming noise in entanglement distribution, Phys. Rev. X **9**, 041042 (2019).
[31] M. Erhard, R. Fickler, M. Krenn, and A. Zeilinger, Twisted photons: new quantum perspectives in high dimensions, Light: Sci. Appl. **7**, 17146 (2018).
[32] D. Cozzolino, B. Da Lio, D. Bacco, and L. K. Oxenløwe, High-dimensional quantum communication: benefits, progress, and future challenges, Adv. Quantum Technol. **2**, 1900038 (2019).
[33] M. Erhard, M. Krenn, and A. Zeilinger, Advances in high-dimensional quantum entanglement, Nat. Rev. Phys. **2**, 365 (2020).
[34] Y. Chi, Y. Yu, Q. Gong, and J. Wang, High-dimensional quantum information processing on programmable integrated photonic chips, Sci. China Inf. Sci. **66**, 180501 (2023).
[35] M. S. Blok, V. V. Ramasesh, T. Schuster, K. OBrien, J.-M. Kreikebaum, D. Dahlen, A. Morvan, B. Yoshida, N. Y. Yao, and I. Siddiqi, Quantum information scrambling on a superconducting qutrit processor, Phys. Rev. X **11**, 021010 (2021).
[36] A. Cervera-Lierta, M. Krenn, A. Aspuru-Guzik, and A. Galda, Experimental high-dimensional Greenberger–Horne–Zeilinger entanglement with superconducting transmon qutrits, Phys. Rev. Appl. **17**, 024062 (2022).
[37] M. Ringbauer, M. Meth, L. Postler, R. Stricker, R. Blatt, P. Schindler, and T. Monz, A universal qudit quantum processor with trapped ions, Nat. Phys. **18**, 1053 (2022).
[38] B. E. Anderson, H. Sosa-Martinez, C. A. Riofrío, I. H. Deutsch, and P. S. Jessen, Accurate and robust unitary transformations of a high-dimensional quantum system, Phys. Rev. Lett. **114**, 240401 (2015).

[39] Y. Fu, W. Liu, X. Ye, Y. Wang, C. Zhang, C. K. Duan, X. Rong, and J. Du, Experimental investigation of quantum correlations in a two-qutrit spin system, Phys. Rev. Lett. **129**, 100501 (2022).

[40] M. Michler, H. Weinfurter, and M. Żukowski, Experiments towards falsification of noncontextual hidden variable theories, Phys. Rev. Lett. **84**, 5457 (2000).

[41] Z. B. Chen, J. W. Pan, Y. D. Zhang, Č. Brukner, and A. Zeilinger, All-versus-nothing violation of local realism for two entangled photons, Phys. Rev. Lett. **90**, 160408 (2003).

[42] Y. H. Kim, Single-photon two-qubit entangled states: Preparation and measurement, Phys. Rev. A **67**, 040301(R) (2003).

[43] H. T. Lim, Y. S. Kim, Y. S. Ra, J. Bae, and Y. H. Kim, Experimental realization of an approximate transpose operation for qutrit systems using a structural physical approximation, Phys. Rev. A **86**, 042334 (2012).

[44] X. M. Hu, W. B. Xing, B. H. Liu, Y. F. Huang, C. F. Li, G. C. Guo, P. Erker, and M. Huber, Efficient generation of high-dimensional entanglement through multipath down-conversion, Phys. Rev. Lett. **125**, 090503 (2020).

[45] X. Wang, X. Zhan, Y. Li, L. Xiao, G. Zhu, D. Qu, Q. Lin, Y. Yu, and P. Xue, Generalized quantum measurements on a higher-dimensional system via quantum walks, Phys. Rev. Lett. **131**, 150803 (2023).

[46] A. Babazadeh, M. Erhard, F. Wang, M. Malik, R. Nouroozi, M. Krenn, and A. Zeilinger, High-dimensional single-photon quantum gates: concepts and experiments, Phys. Rev. Lett. **119**, 180510 (2017).

[47] X. Gao, M. Krenn, J. Kysela, and A. Zeilinger, Arbitrary d-dimensional Pauli X gates of a flying qudit, Phys. Rev. A **99**, 023825 (2019).

[48] X. Gao, M. Erhard, A. Zeilinger, and M. Krenn, Computer-inspired concept for high-dimensional multipartite quantum gates, Phys. Rev. Lett. **125**, 050501 (2020).

[49] Y. Wang, S. Ru, F. Wang, P. Zhang, and F. Li, Experimental demonstration of efficient high-dimensional quantum gates with orbital angular momentum, Quantum Sci. Technol. **7**, 015016 (2022).

[50] P. Imany, J. A. Jaramillo-Villegas, M. S. Alshaykh, J. M. Lukens, O. D. Odele, A. J. Moore, D. E. Leaird, M. Qi, and A. M. Weiner, High-dimensional optical quantum logic in large operational spaces, npj Quantum Inf. **5**, 59 (2019).

[51] F. Brandt, M. Hiekkamäki, F. Bouchard, M. Huber, and R. Fickler, High-dimensional quantum gates using full-field spatial modes of photons, Optica **7**, 98 (2020).

[52] Y. Chi, J. Huang, Z. Zhang, J. Mao, Z. Zhou, X. Chen, C. Zhai, J. Bao, T. Dai, H. Yuan, M. Zhang, D. Dai, B. Tang, Y. Yang, Z. Li, Y. Ding, L. K. Oxenløwe, M. G. Thompson, J. L. O'Brien, Y. Li *et al.*, A programmable qudit-based quantum processor, Nat. Commun. **13**, 1166 (2022).

[53] Q. Zeng, T. Li, X. Song, and X. Zhang, Realization of optimized quantum controlled-logic gate based on the orbital angular momentum of light, Opt. Express **24**, 8186 (2016).

[54] J. Lopes, W. Soares, B. de Lima Bernardo, D. Caetano, and A. Canabarro, Linear optical CNOT gate with orbital angular momentum and polarization, Quantum Info. Proc. **18**, 256 (2019).

[55] H. Ke, S. Fang, and W. Zhang, A versatile device for implementing the optical quantum gates in multiple degrees of freedom, Opt. Laser Technol. **169**, 110137 (2024).

[56] Y. Li, P. C. Humphreys, G. J. Mendoza, and S. C. Benjamin, Resource costs for fault-tolerant linear optical quantum computing, Phys. Rev. X **5**, 041007 (2015).

[57] I. Tzitrin, T. Matsuura, R. N. Alexander, G. Dauphinais, J. E. Bourassa, K. K. Sabapathy, N. C. Menicucci, and I. Dhand, Fault-tolerant quantum computation with static linear optics, PRX Quantum **2**, 040353 (2021).

[58] S. D. Bartlett, H. de Guise, and B. C. Sanders, Quantum encodings in spin systems and harmonic oscillators, Phys. Rev. A **65**, 052316 (2002).

[59] Y. I. Bogdanov, M. V. Chekhova, S. P. Kulik, G. A. Maslennikov, A. A. Zhukov, C. H. Oh, and M. K. Tey, Qutrit state engineering with biphotons, Phys. Rev. Lett. **93**, 230503 (2004).

[60] E. V. Moreva, G. A. Maslennikov, S. S. Straupe, and S. P. Kulik, Realization of four-level qudits using biphotons, Phys. Rev. Lett. **97**, 023602 (2006).

[61] S. Y. Baek and Y. H. Kim, Scalable scheme for entangling multiple ququarts using linear optical elements, Phys. Lett. A **370**, 28 (2007).

[62] M. V. Fedorov, P. A. Volkov, J. M. Mikhailova, S. S. Straupe, and S. P. Kulik, Entanglement of biphoton states: Qutrits and ququarts, New J. Phys. **13**, 083004 (2011).

[63] B. Do, M. L. Stohler, S. Balasubramanian, D. S. Elliott, C. Eash, E. Fischbach, M. A. Fischbach, A. Mills, and B. Zwickl, Experimental realization of a quantum quincunx by use of linear optical elements, J. Opt. Soc. Am. B **22**, 499 (2005).

[64] A. M. Childs, Universal computation by quantum walk, Phys. Rev. Lett. **102**, 180501 (2009).

[65] N. B. Lovett, S. Cooper, M. Everitt, M. Trevers, and V. Kendon, Universal quantum computation using the discrete-time quantum walk, Phys. Rev. A **81**, 042330 (2010).

[66] F. Wang, M. Erhard, A. Babazadeh, M. Malik, M. Krenn, and A. Zeilinger, Generation of the complete four-dimensional Bell basis, Optica **4**, 1462 (2017).

[67] M. Mafu, A. Dudley, S. Goyal, D. Giovannini, M. McLaren, M. J. Padgett, T. Konrad, F. Petruccione, N. Lütkenhaus, and A. Forbes, Higher-dimensional orbital-angular-momentum-based quantum key distribution with mutually unbiased bases, Phys. Rev. A **88**, 032305 (2013).

[68] Y. H. Luo, H. S. Zhong, M. Erhard, X. L. Wang, L. C. Peng, M. Krenn, X. Jiang, L. Li, N. L. Liu, C. Y. Lu *et al.*, Quantum teleportation in high dimensions, Phys. Rev. Lett. **123**, 070505 (2019).

[69] T. Feng, Q. Xu, L. Zhou, M. Luo, W. Zhang, and X. Zhou, Quantum information transfer between a two-level and a four-level quantum systems, Photon. Res. **10**, 2854 (2022).

[70] M. Reck, A. Zeilinger, H. J. Bernstein, and P. Bertani, Experimental realization of any discrete unitary operator, Phys. Rev. Lett. **73**, 58 (1994).